Journal of the Brazilian Society of Mechanical Sciences and Engineering (2019) 41:573
https://doi.org/10.1007/s40430-019-2071-6

TECHNICAL PAPER

Mixed-mode computation of the transient dynamic stress intensity factor for multiple interface cracks

A. Jafari[2] · M. M. Monfared[1] · R. Bagheri[2]

Received: 19 July 2019 / Accepted: 8 November 2019 / Published online: 19 November 2019

Abstract
In this paper, the transient dynamic stress intensity factors are estimated for multiple cracks which are located at the interface between a nonhomogeneous elastic half-plane and an elastic half-plane. The material properties of the nonhomogeneous half-plane vary continuously in the y-direction. First, Laplace and Fourier transforms are applied to reduce the mixed boundary value problem to a system of singular integral equations with Cauchy kernels which are solved numerically. By numerical Laplace inversion technique, the dislocation density on the crack faces is obtained and then transient dynamic stress intensity factors at crack tips have been determined. For validity and accuracy of the method, the results are compared with other references and very good agreement is shown. The influences of nonhomogeneity parameters, crack length, the variation in time and the interaction between of cracks on the transient dynamic stress intensity factors are studied. It is observed that the mode I stress intensity factors decrease regularly with increasing the FG constant and the results are briefly discussed.

Keywords Multiple interface cracks · Two dissimilar half-planes · Mixed-mode transient dynamic stress intensity factors · Functionally graded materials · Dislocation densities

1 Introduction

In recent years, functionally graded materials (FGMs) have been extensively used as coatings to remove the effects of sharp interfaces. Functionally graded structures have been widely introduced and applied to the development of thermal and structural components due to their ability to not only reduce the residual and thermal stresses but increase the bonding strength and toughness as well. In the past decades, the fracture behaviors of FGMs have been investigated by several researchers with various geometries and crack modes, and a brief review of the article is mentioned below.

Delale and Erdogan [1] studied the crack problem in the interfacial zone between two homogeneous half-planes. Hutchinson and Suo [2] reviewed the stress intensity factor of the mixed-mode fracture of an interface crack. The generalized mixed-mode problem for a crack with an arbitrary orientation in FGMs was discussed by Konda and Erdogan [3]. Modes I, II stress intensity factors for two coaxial cracks in an orthotropic plane subjected to a time-harmonic plane wave were obtained by Itou and Haliding [4]. It was shown that the stress intensity factors are dependent on material properties of the media, distance between cracks and the ratio of crack lengths. Ikeda et al. [5] presented the concept of the stress intensity factors of an interface crack between dissimilar materials so that various types of specimens were tested experimentally for investigating the mixed-mode facture toughness criterion of an interface crack. The internal and edge crack problem of an FGM layer attached to an elastic foundation was considered by Kadioğlu et al. [6]. Jiang and Wang [7] studied a finite crack with constant length propagating in an interfacial FGM layer under in-plane loading. The transient response of the internal crack which is perpendicular to the free surfaces in a functionally graded orthotropic strip was considered by Chen et al. [8]. In this analysis, integral transforms and dislocation density functions were employed to reduce the problem to singular

Technical Editor: João Marciano Laredo dos Reis.

✉ M. M. Monfared
mo_m_monfared@yahoo.com

[1] Department of Mechanical Engineering, Hashtgerd Branch, Islamic Azad University, P.O. Box 33615-178, Hashtgerd, Alborz, Iran

[2] Department of Mechanical Engineering, Mechatronics Faculty, Karaj Branch, Islamic Azad University, Karaj, Alborz, Iran

integral equations. A crack located in an orthotropic FG strip under anti-plane impact loading was studied by Feng et al. [9]. The dynamic fracture behavior of a functionally graded coating–substrate system with an internal crack perpendicular to the interface under an in-plane impact load was investigated by Guo et al. [10]. Interface crack located between a graded orthotropic coating and a homogeneous orthotropic substrate using both the singular integral equation and enriched finite element techniques was studied by Dag et al. [11]. The results showed that enriched finite element technique is a strong method for analyzing crack problems. Chen and Liu [12] considered an orthotropic FGM layer under mode III deformation weakened by an internal or an edge crack which was perpendicular to the boundaries of a layer. Wang and Mai [13] provided a periodic array of cracks in an FGM plane under mode I and mode II transient mechanical loading. A crack situated between the two nonhomogeneous layers under mixed-mode transient loading was investigated by Li et al. [14]. The results showed that the weak discontinuity is an important factor affecting the SIFs of the interfacial crack. The mixed-mode fracture problem of orthotropic functionally graded material under mechanical and thermal loading conditions was analyzed by Dag et al. [15]. An elastic isotropic plane weakened by two and three parallel cracks under dynamic loading was examined by Itou [16]. In another paper, the transient response of a homogeneous strip with an internal crack was investigated by Itou [17]. Mixed-mode stress intensity factors in an orthotropic functionally graded plane, a half-plane and a strip containing multiple curved cracks under static loading were analyzed by Monfared and Ayatollahi [18], Monfared and Bagheri [19], Monfared et al. [20, 21], respectively.

The transient dynamic mixed-mode stress intensity factors presented in this paper are obtained using distributed dislocation method. First, Fourier and Laplace transforms are used to convert the two partial differential equations in each region into a system of singular integral equations with Cauchy-type singularity. These equations are solved numerically by means of the Lobatto–Chebyshev collocation method [21] and of the Stehfest method [22] to obtain the dislocation densities on the crack faces. Then, dislocation densities are applied to calculate the transient mixed-mode stress intensity factors at crack tips for multiple interface cracks. Attention will be paid to the influences of the time variation, the gradient of the material property and also crack interactions on the transient dynamic stress intensity factors.

2 Dislocation solution

We consider an FGM half-plane bonded to a homogeneous half-plane as shown in Fig. 1. The edge dislocations located between the two dissimilar half-planes to analyze the stress field and to determine the SIFs at crack tips.

Under the in-plane deformation, the constitutive relation of FGM medium whose mechanical properties vary continuously along the y-direction can be written as

$$\begin{aligned}
\sigma_{xx}(x,y,t) &= \frac{\mu(y)}{\kappa-1}\left[(\kappa+1)\frac{\partial u}{\partial x}+(3-\kappa)\frac{\partial v}{\partial y}\right],\\
\sigma_{yy}(x,y,t) &= \frac{\mu(y)}{\kappa-1}\left[(3-\kappa)\frac{\partial u}{\partial x}+(\kappa+1)\frac{\partial v}{\partial y}\right],\\
\sigma_{xy}(x,y,t) &= \mu(y)\left(\frac{\partial u}{\partial y}+\frac{\partial v}{\partial x}\right).
\end{aligned} \tag{1}$$

In the above equation, $\mu(y)$ and κ stand for the shear modulus of elasticity and Kolosov constant, respectively. The Kolosov constant is $\kappa=\frac{3-\upsilon}{1+\upsilon}$ for plane stress and $\kappa=3-4\upsilon$ for plane strain situations, where υ is the Poisson's ratio of material. Due to the complexity of mathematics involved, the distribution of mechanical properties of FGMs may be approximated by an exponential function (Konda and Erdogan [3], Kadioğlu et al. [6], Chen and Liu [12] and Sourki et al. [23]) as follows:

$$\mu(y)=\mu_0 e^{\beta y} \tag{2}$$

where μ_0 is elastic constant in the homogeneous half-plane and β is the gradient parameter to describe the inhomogeneous material distribution. By virtue of Eq. (1) and the equations of motion, $\frac{\partial\sigma_{xx}}{\partial x}+\frac{\partial\sigma_{xy}}{\partial y}=\rho(y)\frac{\partial^2 u}{\partial t^2}$ and $\frac{\partial\sigma_{xy}}{\partial x}+\frac{\partial\sigma_{yy}}{\partial y}=\rho(y)\frac{\partial^2 v}{\partial t^2}$, we can obtain the governing equations as follows:

$$\begin{aligned}
&(\kappa+1)\frac{\partial^2 u}{\partial x^2}+2\frac{\partial^2 v}{\partial x\partial y}+(\kappa-1)\frac{\partial^2 u}{\partial y^2}\\
&\quad+\beta(\kappa-1)\left(\frac{\partial u}{\partial y}+\frac{\partial v}{\partial x}\right)=c^2(\kappa-1)\frac{\partial^2 u}{\partial t^2},\\
&(\kappa-1)\frac{\partial^2 v}{\partial x^2}+2\frac{\partial^2 u}{\partial x\partial y}+(\kappa+1)\frac{\partial^2 v}{\partial y^2}\\
&\quad+\beta(\kappa+1)\frac{\partial v}{\partial y}+\beta(3-\kappa)\frac{\partial u}{\partial x}=c^2(\kappa-1)\frac{\partial^2 v}{\partial t^2},
\end{aligned} \tag{3}$$

$y\geq 0$.

In the above equation, it is assumed that the mass density of the FGM medium varies exponentially along the y-axis

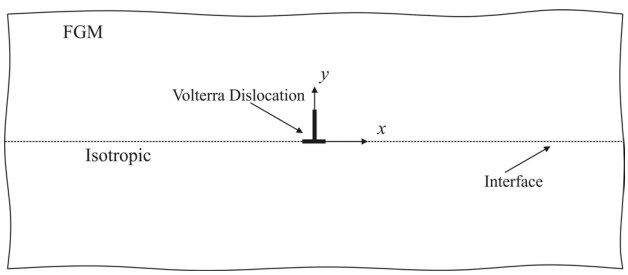

Fig. 1 Schematic of dislocation between two half-planes

with $\rho(y) = \rho_0 e^{\beta y}$, where ρ_0 is the density at $y = 0$ and $c = \frac{1}{C}$, $C = \sqrt{\mu_0/\rho_0}$ is the shear wave speed of the material. Note that the material gradient parameter has been considered identical in mass density and shear modulus but in reality, it may be different in mass density and shear modulus (see Ref. [24]). The partial differential equations for the homogeneous half-plane can be obtained by substituting 0 for β in Eq. (3). Let Volterra edge dislocations with time-dependent Burgers vector be situated at the interface (Fig. 1). The dislocation cut created along the positive direction of the x-axis at the interface materials, while glide and climb of the edge dislocation are represented $b_x(t)$ and $b_y(t)$, respectively. Therefore, the displacement conditions at the dislocation path and the continuity of traction on the dislocation cut are:

$$\begin{aligned} &u(x,0^+,t) - u(x,0^-,t) = b_x(t)H(x),\\ &v(x,0^+,t) - v(x,0^-,t) = b_y(t)H(x),\\ &\sigma_{yy}(x,0^+,t) = \sigma_{yy}(x,0^-,t),\\ &\sigma_{xy}(x,0^+,t) = \sigma_{xy}(x,0^-,t). \end{aligned} \tag{4}$$

where $H(.)$ is the Heaviside step function. By applying Laplace transform to Eq. (3) with the initial values of the displacements and their time-derivatives assumed to be zero, the following equations are obtained:

$$\begin{aligned} &(\kappa+1)\frac{\partial^2 u^*}{\partial x^2} + 2\frac{\partial^2 v^*}{\partial x \partial y} + (\kappa-1)\frac{\partial^2 u^*}{\partial y^2}\\ &+ \beta(\kappa-1)\left(\frac{\partial u^*}{\partial y} + \frac{\partial v^*}{\partial x}\right) = c^2(\kappa-1)s^2 u^*,\\ &(\kappa-1)\frac{\partial^2 v^*}{\partial x^2} + 2\frac{\partial^2 u^*}{\partial x \partial y} + (\kappa+1)\frac{\partial^2 v^*}{\partial y^2}\\ &+ \beta(\kappa+1)\frac{\partial v^*}{\partial y} + \beta(3-\kappa)\frac{\partial u^*}{\partial x} = c^2(\kappa-1)s^2 v^*. \end{aligned} \tag{5}$$

where the superscript * denotes the Laplace transform, s is Laplace variable at the time transform domain. Applying Fourier transform to Eq. (5) with respect to x and assuming that displacement fields decay rapidly as $x \to \infty$, Eq. (5) can be rewritten as

$$\begin{aligned} &(\kappa-1)\frac{\mathrm{d}^2 U^*}{\mathrm{d}y^2} + \beta(\kappa-1)\frac{\mathrm{d}U^*}{\mathrm{d}y} + 2i\xi\frac{\mathrm{d}V^*}{\mathrm{d}y}\\ &+ i\xi\beta(\kappa-1)V^* - [\xi^2(\kappa+1) + c^2(\kappa-1)s^2]U^* = 0,\\ &(\kappa+1)\frac{\mathrm{d}^2 V^*}{\mathrm{d}y^2} + \beta(\kappa+1)\frac{\mathrm{d}V^*}{\mathrm{d}y} + 2i\xi\frac{\mathrm{d}U^*}{\mathrm{d}y}\\ &+ i\xi\beta(3-\kappa)U^* - [\xi^2(\kappa-1) + c^2(\kappa-1)s^2]V^* = 0, \quad y \geq 0, \end{aligned} \tag{6}$$

where $i = \sqrt{-1}$, ξ is Fourier variable and U and V are Fourier transforms of displacement components u and v, respectively. The general solutions of Eq. (6) can be expressed as follows:

$$\begin{aligned} U^*(\xi,y,s) &= A_1 e^{\lambda_1 y} + A_2 e^{\lambda_2 y} + A_3 e^{\lambda_3 y} + A_4 e^{\lambda_4 y},\\ V^*(\xi,y,s) &= ia_{11}A_1 e^{\lambda_1 y} + ia_{21}A_2 e^{\lambda_2 y}\\ &\quad + ia_{31}A_3 e^{\lambda_3 y} + ia_{41}A_4 e^{\lambda_4 y}, \quad y \geq 0, \end{aligned} \tag{7}$$

where A_j, $j = 1,2,3,4$ are the unknown functions. The characteristic roots λ_j, $j = 1,2,3,4$ and the functions a_{1j}, $j = 1,2,3,4$ are given as

$$\begin{aligned} &\lambda_1 = \frac{1}{2}\left[-\beta - \sqrt{\beta^2 - 2\Delta_1 + 2\sqrt{\Delta_1^2 - 4\Delta_2}}\right],\\ &\lambda_2 = \frac{1}{2}\left[-\beta - \sqrt{\beta^2 - 2\Delta_1 - 2\sqrt{\Delta_1^2 - 4\Delta_2}}\right], \quad \mathrm{Re}(\lambda_1,\lambda_2) < 0\\ &\lambda_3 = \frac{1}{2}\left[-\beta + \sqrt{\beta^2 - 2\Delta_1 + 2\sqrt{\Delta_1^2 - 4\Delta_2}}\right],\\ &\lambda_4 = \frac{1}{2}\left[-\beta + \sqrt{\beta^2 - 2\Delta_1 - 2\sqrt{\Delta_1^2 - 4\Delta_2}}\right], \quad \mathrm{Re}(\lambda_3,\lambda_4) > 0\\ &a_{j1} = \frac{(\kappa-1)\lambda_j^2 + \beta(\kappa-1)\lambda_j - [\xi^2(\kappa+1) + c^2(\kappa-1)s^2]}{\xi[2\lambda_j + \beta(\kappa-1)]},\\ &j = 1,2,3,4 \end{aligned} \tag{8}$$

where Δ_1 and Δ_2 are $\Delta_1 = -2\xi^2 - \frac{2\kappa c^2 s^2}{\kappa+1}$, $\Delta_2 = \xi^4 + \frac{2\kappa c^2 s^2 \xi^2}{\kappa+1} + \frac{c^4 s^4(\kappa-1)}{\kappa+1} - \xi^2\beta^2\frac{(\kappa-3)}{\kappa+1}$. Following a very similar procedure of applying Fourier transform, the solution for the homogeneous half-plane can be expressed as

$$\begin{aligned} U^*(\xi,y,s) &= C_1 e^{r_1 y} + C_2 e^{r_2 y} + C_3 e^{r_3 y} + C_4 e^{r_4 y},\\ V^*(\xi,y,s) &= ib_{11}C_1 e^{r_1 y} + ib_{21}C_2 e^{r_2 y}\\ &\quad + ib_{31}C_3 e^{r_3 y} + ib_{41}C_4 e^{r_4 y}, \quad y \leq 0. \end{aligned} \tag{9}$$

where C_j, $j = 1,2,3,4$ are the unknown functions. The characteristic roots r_j, $j = 1,2,3,4$ and b_{1j}, $j = 1,2,3,4$ are given in the following form:

$$\begin{aligned} &r_1 = \sqrt{\xi^2 + c^2 s^2}, \quad r_2 = \sqrt{\xi^2 + c^2 s^2 \frac{\kappa-1}{\kappa+1}}, \quad \mathrm{Re}(r_1,r_2) > 0\\ &r_3 = -\sqrt{\xi^2 + c^2 s^2}, \quad r_4 = -\sqrt{\xi^2 + c^2 s^2 \frac{\kappa-1}{\kappa+1}}, \quad \mathrm{Re}(r_3,r_4) < 0\\ &b_{j1} = \frac{(\kappa-1)r_j^2 - [\xi^2(\kappa+1) + c^2(\kappa-1)s^2]}{2\xi r_j}, \quad j = 1,2,3,4 \end{aligned} \tag{10}$$

The displacements in Eq. (7) while $y \to \infty$ and also the displacements in Eq. (9) while $y \to -\infty$ must be limited. Thus, the unknown functions A_3, A_4 in Eq. (7) and C_3, C_4 in Eq. (9) become zero. Employing the inverse Fourier transform, the displacement fields in Eqs. (7) and (9) lead to

$$\begin{cases} u^*(x,y,s) = \frac{1}{2\pi}\int_{-\infty}^{\infty}(A_1 e^{\lambda_1 y} + A_2 e^{\lambda_2 y})\, e^{i\xi x}\mathrm{d}\xi, \\ v^*(x,y,s) = \frac{i}{2\pi}\int_{-\infty}^{\infty}(a_{11}A_1 e^{\lambda_1 y} + a_{21}A_2 e^{\lambda_2 y})\, e^{i\xi x}\mathrm{d}\xi, \quad y \geq 0, \end{cases}$$

$$\begin{cases} u^*(x,y,s) = \frac{1}{2\pi}\int_{-\infty}^{\infty}(C_1 e^{r_1 y} + C_2 e^{r_2 y})\, e^{i\xi x}\mathrm{d}\xi, \\ v^*(x,y,s) = \frac{i}{2\pi}\int_{-\infty}^{\infty}(b_{11}C_1 e^{r_1 y} + b_{21}C_2 e^{r_2 y})\, e^{i\xi x}\mathrm{d}\xi, \quad y \leq 0. \end{cases} \tag{11}$$

Using Eqs. (1), (2) and (11), the stress fields in two regions become

$$\begin{aligned}
\sigma_{xx}^*(x,y,s) &= \frac{i\mu_0 e^{\beta y}}{2\pi(\kappa-1)}\int_{-\infty}^{\infty}\sum_{j=1}^{2} a_{j2}A_j e^{\lambda_j y} e^{i\xi x}\mathrm{d}\xi, \\
\sigma_{yy}^*(x,y,s) &= \frac{i\mu_0 e^{\beta y}}{2\pi(\kappa-1)}\int_{-\infty}^{\infty}\sum_{j=1}^{2} a_{j3}A_j e^{\lambda_j y} e^{i\xi x}\mathrm{d}\xi, \\
\sigma_{xy}^*(x,y,s) &= \frac{\mu_0 e^{\beta y}}{2\pi}\int_{-\infty}^{\infty}\sum_{j=1}^{2} a_{j4}A_j e^{\lambda_j y} e^{i\xi x}\mathrm{d}\xi, \quad y \geq 0, \\
\sigma_{xx}^*(x,y,s) &= \frac{i\mu_0}{2\pi(\kappa-1)}\int_{-\infty}^{\infty}\sum_{j=1}^{2} b_{j2}C_j e^{r_j y} e^{i\xi x}\mathrm{d}\xi, \\
\sigma_{yy}^*(x,y,s) &= \frac{i\mu_0}{2\pi(\kappa-1)}\int_{-\infty}^{\infty}\sum_{j=1}^{2} b_{j3}C_j e^{r_j y} e^{i\xi x}\mathrm{d}\xi, \\
\sigma_{xy}^*(x,y,s) &= \frac{\mu_0}{2\pi}\int_{-\infty}^{\infty}\sum_{j=1}^{2} b_{j4}C_j e^{r_j y} e^{i\xi x}\mathrm{d}\xi, \quad y \leq 0.
\end{aligned} \tag{12}$$

where the functions $a_{j2}, a_{j3}, a_{j4}, b_{j2}, b_{j3}, b_{j4}\, j = 1, 2.$ are given as

$$\begin{aligned}
a_{j2} &= (\kappa+1)\xi + (3-\kappa)\, a_{j1}\lambda_j, \\
a_{j3} &= (3-\kappa)\xi + (\kappa+1)\, a_{j1}\lambda_j, \\
a_{j4} &= \lambda_j - \xi a_{j1}, \\
b_{j2} &= (\kappa+1)\xi + (3-\kappa)\, b_{j1} r_j, \\
b_{j3} &= (3-\kappa)\xi + (\kappa+1)\, b_{j1} r_j, \\
b_{j4} &= r_j - \xi b_{j1}.
\end{aligned} \tag{13}$$

The unknown coefficients in Eq. (12) $(A_j, C_j, j = 1, 2)$ may be obtained by taking the Fourier and Laplace transforms of Eq. (4) and applying the resultant expression to Eq. (12) as follows:

$$\begin{aligned}
A_1 &= [A_{11}b_x(s) + iA_{12}b_y(s)](\pi\delta(\xi) - i/\xi) \\
A_2 &= [A_{21}b_x(s) + iA_{22}b_y(s)](\pi\delta(\xi) - i/\xi) \\
C_1 &= [C_{11}b_x(s) + iC_{12}b_y(s)](\pi\delta(\xi) - i/\xi) \\
C_2 &= [C_{21}b_x(s) + iC_{22}b_y(s)](\pi\delta(\xi) - i/\xi)
\end{aligned} \tag{14}$$

where $\delta(.)$ is the Dirac delta function and $A_{ij}, C_{ij},\ i,j = 1, 2.$ are given in "Appendix 1." Substituting unknown functions (14) into Eq. (12), the stress components in the homogeneous half-plane after some manipulations yield

$$\begin{aligned}
\sigma_{xx}^*(x,y,s) &= \frac{\mu_0}{2\pi(\kappa-1)}\int_{-\infty}^{\infty}\frac{e^{i\xi x}}{\xi}[(b_{12}C_{11}e^{r_1 y} + b_{22}C_{21}e^{r_2 y})\, b_x(s) + i(b_{12}C_{12}e^{r_1 y} + b_{22}C_{22}e^{r_2 y})b_y(s)]\,\mathrm{d}\xi, \\
\sigma_{yy}^*(x,y,s) &= \frac{\mu_0}{2\pi(\kappa-1)}\int_{-\infty}^{\infty}\frac{e^{i\xi x}}{\xi}[(b_{13}C_{11}e^{r_1 y} + b_{23}C_{21}e^{r_2 y})\, b_x(s) + i(b_{13}C_{12}e^{r_1 y} + b_{23}C_{22}e^{r_2 y})\, b_y(s)]\,\mathrm{d}\xi, \\
\sigma_{xy}^*(x,y,s) &= \frac{\mu_0}{2\pi}\int_{-\infty}^{\infty}\frac{-ie^{i\xi x}}{\xi}[(b_{14}C_{11}e^{r_1 y} + b_{24}C_{21}e^{r_2 y})\, b_x(s) + i(b_{14}C_{12}e^{r_1 y} + b_{24}C_{22}e^{r_2 y})\, b_y(s)]\,\mathrm{d}\xi.
\end{aligned} \tag{15}$$

To evaluate the stress components numerically, the integrals in Eq. (15) can be split into odd and even parts to arrive at

$$\begin{aligned}
\sigma_{xx}^*(x,y,s) &= \int_0^{\infty} f_{xx}(x,y,s,\xi)\,\mathrm{d}\xi, \\
\sigma_{yy}^*(x,y,s) &= \int_0^{\infty} f_{yy}(x,y,s,\xi)\,\mathrm{d}\xi, \\
\sigma_{xy}^*(x,y,s) &= \int_0^{\infty} f_{xy}(x,y,s,\xi)\,\mathrm{d}\xi
\end{aligned} \tag{16}$$

where $f_{ij}(x,y,s,\xi), i,j \in \{x,y\}$ are defined as follows:

$$\begin{aligned}
f_{xx}(x,y,s) &= \frac{\mu_0}{\pi(\kappa-1)\xi}[(b_{12}C_{11}e^{r_1 y} + b_{22}C_{21}e^{r_2 y})\cos(\xi x)\, b_x(s) - (b_{12}C_{12}e^{r_1 y} + b_{22}C_{22}e^{r_2 y})\sin(\xi x)\, b_y(s)], \\
f_{yy}(x,y,s) &= \frac{\mu_0}{\pi(\kappa-1)\xi}[(b_{13}C_{11}e^{r_1 y} + b_{23}C_{21}e^{r_2 y})\cos(\xi x)\, b_x(s) - (b_{13}C_{12}e^{r_1 y} + b_{23}C_{22}e^{r_2 y})\sin(\xi x)\, b_y(s)], \\
f_{xy}(x,y,s) &= \frac{\mu_0}{\pi\xi}[(b_{14}C_{11}e^{r_1 y} + b_{24}C_{21}e^{r_2 y})\sin(\xi x)\, b_x(s) + (b_{14}C_{12}e^{r_1 y} + b_{24}C_{22}e^{r_2 y})\cos(\xi x)\, b_y(s)].
\end{aligned} \tag{17}$$

The integrals in Eq. (16) are unbounded for points in the vicinity of dislocation. Thus, the singular behavior of the kernels f_{ij} is determined by asymptotic values of f_{ij} for $\xi \to \infty$ which may be shown as follows:

$$f_{ij}(x,y,s,\xi) = \underbrace{f_{ij\infty}(x,y,s,\xi)}_{\text{Singular Part}} + \underbrace{\left[f_{ij}(x,y,s,\xi) - f_{ij\infty}(x,y,s,\xi)\right]}_{\text{Nonsingular Part}},$$
$$i,j \in \{x,y\}. \tag{18}$$

When $\xi \to \infty$, the asymptotic values of f_{ij} in Eq. (17) can be expressed as

$$\begin{aligned}
f_{xx\infty}(x,y,s) &= -\frac{2\mu_0}{\pi(\kappa+1)}[(2+\xi y)\, e^{\xi y}\cos(\xi x)\, b_x(s) \\
&\quad + (1+\xi y)\, e^{\xi y}\sin(\xi x)\, b_y(s)], \\
f_{yy\infty}(x,y,s) &= \frac{2\mu_0}{\pi(\kappa+1)}[\xi y e^{\xi y}\cos(\xi x)\, b_x(s) \\
&\quad - (1-\xi y)\, e^{\xi y}\sin(\xi x)\, b_y(s)], \\
f_{xy\infty}(x,y,s) &= \frac{2\mu_0}{\pi(\kappa+1)}[-(1+\xi y)\, e^{\xi y}\sin(\xi x)\, b_x(s) \\
&\quad + \xi y e^{\xi y}\cos(\xi x)\, b_y(s)].
\end{aligned} \tag{19}$$

The stress components (16) by view of Eqs. (18) and (19) are as follows:

$$\begin{aligned}
\sigma^*_{xx}(x,y,s) &= \frac{2\mu_0}{\pi(\kappa+1)}\frac{y(3x^2+y^2)\, b_x(s) + x(y^2-x^2)\, b_y(s)}{(x^2+y^2)^2} + \int_0^\infty [f_{xx}(x,y,s,\xi) - f_{xx\infty}(x,y,s,\xi)]\, \mathrm{d}\xi, \\
\sigma^*_{yy}(x,y,s) &= \frac{2\mu_0}{\pi(\kappa+1)}\frac{y(y^2-x^2) b_x(s) - x(x^2+3y^2)\, b_y(s)}{(x^2+y^2)^2} + \int_0^\infty [f_{yy}(x,y,s,\xi) - f_{yy\infty}(x,y,s,\xi)]\, \mathrm{d}\xi, \\
\sigma^*_{xy}(x,y,s) &= \frac{2\mu_0}{\pi(\kappa+1)}\frac{x(y^2-x^2)\, b_x(s) + y(y^2-x^2)\, b_y(s)}{(x^2+y^2)^2} + \int_0^\infty [f_{xy}(x,y,s,\xi) - f_{xy\infty}(x,y,s,\xi)]\, \mathrm{d}\xi.
\end{aligned} \tag{20}$$

The integrals in Eq. (20) are bounded and may be evaluated by numerical methods.

3 Analysis of multiple interface cracks

The solutions of edge dislocations obtained in the preceding section are used to construct integral equations for the analysis of a dissimilar half-planes weakened by N interface cracks. An interface crack configuration may be described in parametric form as

$$\begin{aligned}
&x_i(p) = x_{0i} + p a_i, \\
&y_i(p) = 0, \qquad -1 \le p \le 1, \quad i \in \{1,2,\ldots N\}.
\end{aligned} \tag{21}$$

where $(x_{0i}, 0)$, a_i are the coordinates of center and half-length of the ith cracks, respectively. The components of traction on the face of ith crack at a point with coordinates (x_i, y_i) due to the presence of above-mentioned distribution of dislocations on all N cracks yield

$$\begin{aligned}
\sigma^*_{yy}(x_i(p), y_i(p), s) &= \sum_{k=1}^{N} a_k \int_{-1}^{1} \Big[k^{11}_{yyik}(p,q,s) b_{xk}(q,s) \\
&\quad + k^{12}_{yyik}(p,q,s) b_{yk}(q,s)\Big]\mathrm{d}q, \\
\sigma^*_{xy}(x_i(p), y_i(p), s) &= \sum_{k=1}^{N} \int_{-1}^{1} a_k \Big[k^{11}_{xyik}(p,q,s) b_{xk}(q,s) \\
&\quad + k^{12}_{xyik}(p,q,s) b_{yk}(q,s)\Big]\mathrm{d}q, \\
&i = 1,2,\ldots,N, \ -1 \le p \le 1.
\end{aligned} \tag{22}$$

where $b_{xk}(q, s)$ and $b_{yk}(q, s)$ are the Laplace transforms of the dislocation density functions on the face of k-th crack, $k^{lm}_{ik}, l = 1, m = 1, 2, i, k = x, y$ are coefficients of $b_x(s)$ and $b_y(s)$ in Eq. (20). The kernels in Eq. (22) exhibit Cauchy-type singularity for $i = k$ as $q \to p$ and may be expressed as

$$\begin{aligned}
k^{kl}_{rtii}(p,q,s) &= -\frac{2\mu_0}{\pi a_i(\kappa+1)(p-q)} \\
&\quad + \sum_{m=0}^{\infty} a_{kl,mi}(q,s)(p-q)^m \\
&k,l \in \{1,2\}, \ t = y, \ r \in \{x,y\}.
\end{aligned} \tag{23}$$

The singular term of the above equation is obtained by means of the Taylor series expansion of $x_i(p)$ and $y_i(p)$in the vicinity of q. In view of Bueckner's superposition theorem (Bueckner [25]), the left-hand sides of Eq. (22) are the traction components on the presumed face of a crack with opposite sign in the uncracked two dissimilar half-planes subjected to external applied loads. For interface cracks, displacement field is single-valued out of a crack face. Hence,

Eq. (22) should be complimented with the following closure conditions:

$$\int_{-1}^{1} b_{kj}(q,s)\mathrm{d}q = 0, \quad k \in \{x,y\}, j \in \{1,\ldots,N\}. \tag{24}$$

The stress fields near a crack tip exhibit square-root singularity. Thus, dislocation densities are taken as follows:

$$b_{ki}(q,s) = \frac{g_{ki}(q,s)}{\sqrt{1-q^2}}, \quad k \in \{x,y\}, \quad -1 < q < 1, \quad i \in \{1,2,\ldots,N\}. \tag{25}$$

By replacing Eq. (25) into Eqs. (22) and (24), and using the Lobatto–Chebyshev integration formula, the discretization singular integral equations lead to

$$\int_{-1}^{1} k^{1h}_{myij}(p_l,q,s)\frac{g_{ij}(q,s)}{\sqrt{1-q^2}}\mathrm{d}q = \frac{\pi}{n-1}\sum_{r=1}^{n} e_r k^{1h}_{myij}(p_l,q,s)g_{ij}(q_r,s), \quad m \in \{x,y\}, h \in \{1,2\}. \tag{26}$$

where the collocation points are chosen as $q_r = \cos[\frac{(r-1)\pi}{n-1}]$, $r = 1,2,\ldots,n$ and $p_l = \cos[\frac{(2l-1)\pi}{2(n-1)}]$, $l = 1,2,\ldots,n-1$, e_r=0.5 for r=1, n and e_r=1 for $1<r<n$.

The modes I and II stress intensity factors (SIFs) are defined by Baghestani et al. [26] as follows:

$$k_I(s) = \lim_{r\to 0}\sqrt{2r}\sigma_{yy}(r,\theta,s), \quad k_{II}(s) = \lim_{r\to 0}\sqrt{2r}\sigma_{xy}(r,\theta,s). \tag{27}$$

where r is the distance from the crack tip, θ=0 is right and $\theta=\pi$ is left crack tips, respectively. By substituting Eqs. (23) and (25) into Eq. (22) and resultant equations into Eq. (27), the SIFs at the tips of ith crack in terms of dislocation densities lead to

$$\begin{aligned} k_{Ii}(s) &= -\frac{2\mu_0\eta}{\kappa+1}\sqrt{a_i}g_{yi}(\eta,s), \\ k_{IIi}(s) &= -\frac{2\mu_0\eta}{\kappa+1}\sqrt{a_i}g_{xi}(\eta,s), \quad i \in \{1,2,\ldots N\}. \end{aligned} \tag{28}$$

where $\eta = 1$ is the right crack tip and $\eta = -1$ is the left crack tip. The numerical inversion of the Laplace transform is carried out based on the algorithm developed by Stehfest [22] such as

$$k_j(t) \approx \frac{\ln 2}{t}\sum_{m=1}^{M} H_m k_j\left(\frac{\ln 2}{t}m\right), \quad j \in \{I,II\}, \quad t > 0. \tag{29}$$

where M is a chosen positive even number, and H_m is given by

$$H_m = (-1)^{\frac{M}{2}+m}\sum_{j=[0.5(m+1)]}^{\min\left(\frac{M}{2},m\right)} \frac{j^{\frac{M}{2}}(2j)!}{\left(\frac{M}{2}-j\right)!j!(j-1)!(m-j)!(2j-m)!}. \tag{30}$$

In the above equation, [.] signifies the integer part of the quantity.

4 Results and discussion

In this section, some examples are solved to show the applicability of the distributed dislocation technique for any number of interface cracks. First, to validate this method, we choose the two materials to be identical. Under this condition, the bi-material solution should reduce to the solution for homogeneous materials. The number of points for the inversion of Laplace transform, using Stehfest method, is M = 10. In all the following examples, plane strain conditions with Poisson's ratio $\upsilon = 0.3$, modulus of elasticity $E_0 = 200$ GPa and mass density $\rho_0 = 7840$ kg/m^3 are assumed.

A single crack with length $2a = 2$ cm which is located in the homogeneous materials is shown in Fig. 2 under uniform normal step function traction along the crack face. The variations in the dimensionless stress intensity factors $k(t)/k_0$ versus the dimensionless time t/t_0 are plotted in Fig. 3, where t_0 is $t_0 = a\sqrt{\rho_0/\mu_0}$ and k_0 is the static value of SIF for a single crack in a homogenous plane under static normal traction σ_0. It can be seen from Fig. 3 that very good agreement has been obtained between the present method and the papers published by Sih and Embley [27] and Mottale et al. [28].

In the next example, a single crack located between two dissimilar materials with length $2a = 2$ cm under uniform normal and shear step function traction is shown in Figs. 4 and 5, respectively. The normalized modes I and II transient dynamic stress intensity factors for different dimensionless nonhomogeneity parameters $\beta a = -1.0, \beta a = -0.5, \beta a = 0.5, \beta a = 1.0$ are plotted

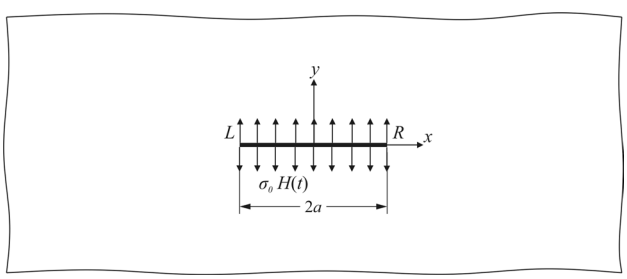

Fig. 2 Geometry of a single crack in homogeneous materials subjected to normal step function traction

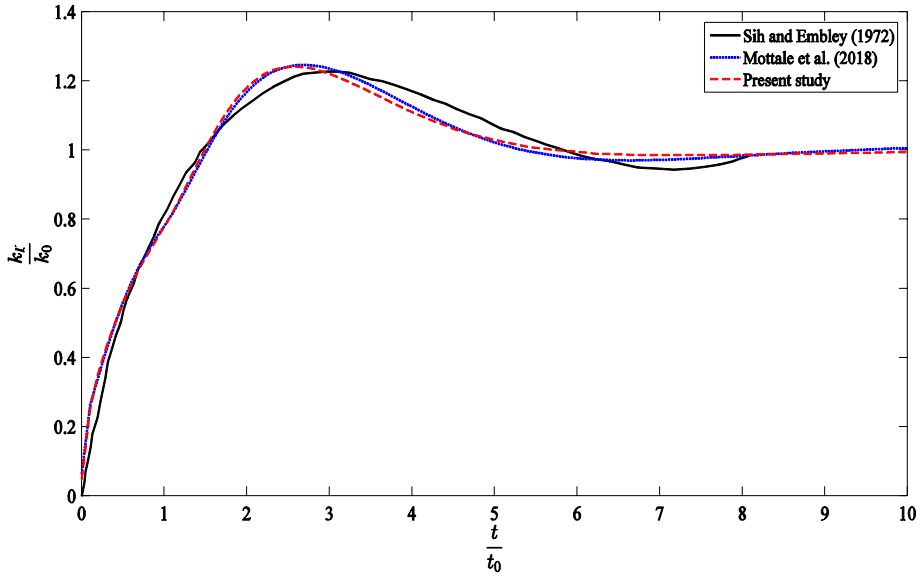

Fig. 3 Comparison of normalized mode I transient DSIFs versus dimensionless time for a homogeneous plane

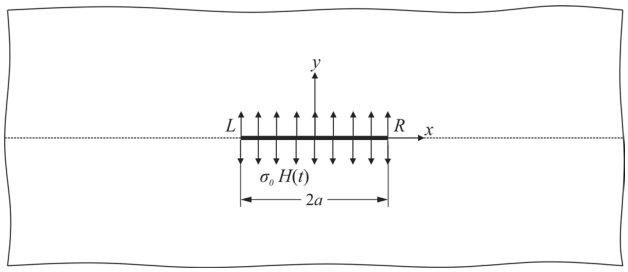

Fig. 4 Geometry of a single crack located between two dissimilar materials subjected to normal step function traction

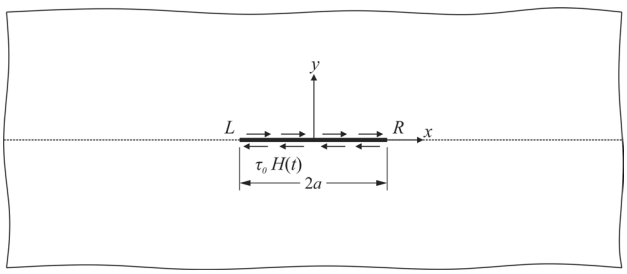

Fig. 5 Geometry of a single crack located between two dissimilar materials subjected to shear step function traction

in Figs. 6 and 7 for normal traction and in Figs. 8 and 9 for shear traction, respectively. DSIFs are normalized by $k_0 = \sigma_0\sqrt{a}$ for normal traction and $k_0 = \tau_0\sqrt{a}$ for shear traction where a is the half-length of crack.

The general feature of these curves is that the transient DSIF varies with time from its initial zero value to a steady state. DSIFs at the left crack tip are the same as those at the right crack tip in mode I under normal traction (Fig. 6) while for mode II, DSIFs at left crack tip and right crack tip are differences with a negative sign (Fig. 7). This trend for DSIFs is reverse under shear traction. With the increase in material gradient parameter βa, the upper side of the half-plane becomes stiffer than the lower side of the half-plane. Then, both the peak and steady values of the mode I DSIFs in normal loading and also mode II DSIFs in shear loading at crack tips decrease regularly. Also note that due to the nonhomogeneity of the medium, the stress intensity factors exhibit mixed-mode condition even though the loading is of one mode.

In the next example, the dimensionless modes I and II transient dynamic stress intensity factors with different Poisson's ratios $\upsilon = 0.25, 0.35, 0.45$ and nonhomogeneous parameter $\beta a = 0.5$ for a single crack located between two dissimilar half-planes under uniform shear traction (Fig. 5) are depicted in Figs. 10 and 11. It can be seen that the Poisson ratio υ has only a negligible influence on the transient dynamic stress intensity factors and also the lack of symmetry with respect to y-axis produces mode I stress intensity factors even where cracks are subjected to shear traction.

To study the interaction of multiple cracks, we consider two cracks situated between two dissimilar half-planes loaded by uniform tractions, which are shown in Fig. 12. The interaction between two cracks with two dimensionless nonhomogeneity parameters $\beta a = 0.5, 1.0$ and dimensionless distance $d/a = 1.05$ is studied in Figs. 13 and 14 for mode I and II, respectively. Due to the symmetry of problem with respect to the y-axis, DSIFs in mode I at tips L_1, R_1 are equal to those at R_2, L_2, respectively. The variation in DSIFs at tips L_1, R_2 is much higher than that at tips R_1, L_2, because these tips have stronger interaction than tips R_1, L_2. Also, it can be observed that the magnitudes of DSIFs for mode I decrease with increase in the nonhomogeneity parameter.

We consider two equal-length cracks L_1R_1 and L_2R_2 as shown in Fig. 12 again. Variations in the normalized modes I

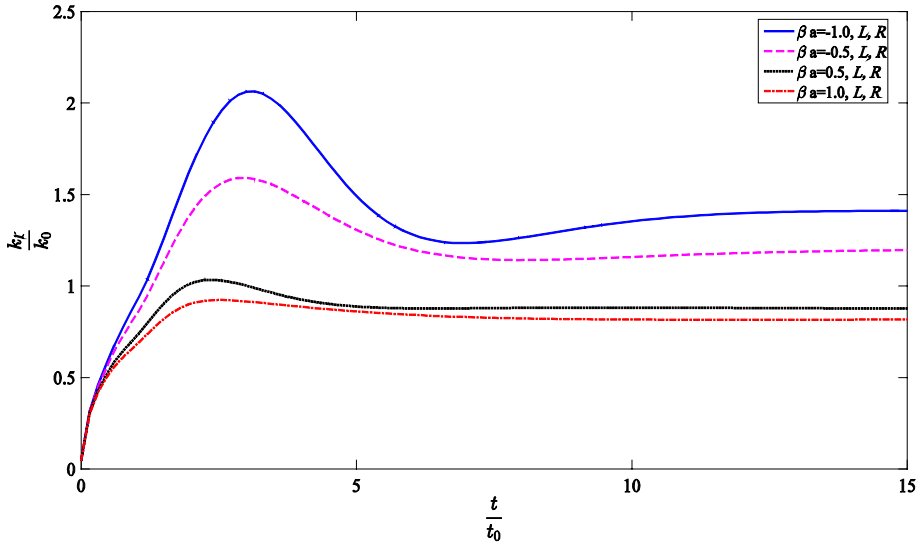

Fig. 6 Variations in normalized mode I transient DSIFs of a single interface crack for different dimensionless nonhomogeneity parameters under normal traction

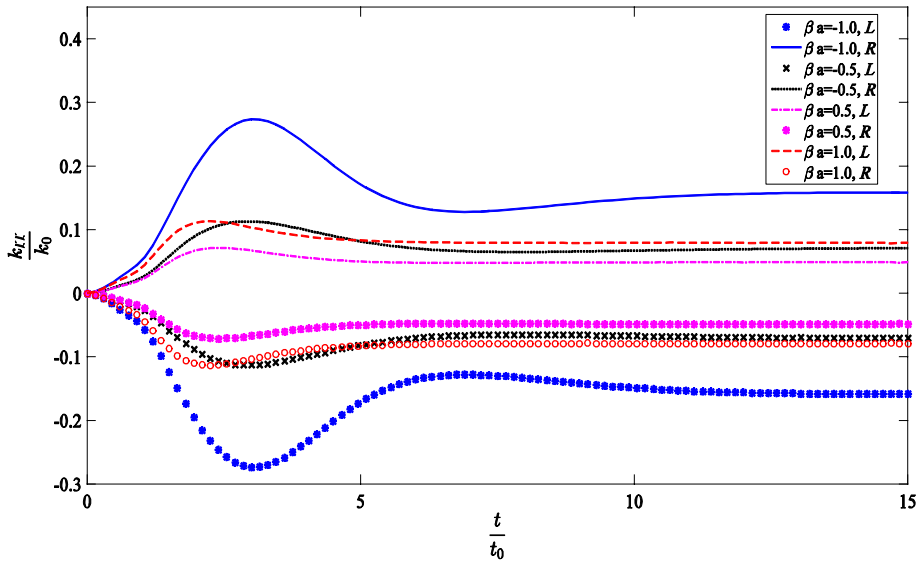

Fig. 7 Variations in normalized mode II transient DSIFs of a single interface crack for different dimensionless nonhomogeneity parameters under normal traction

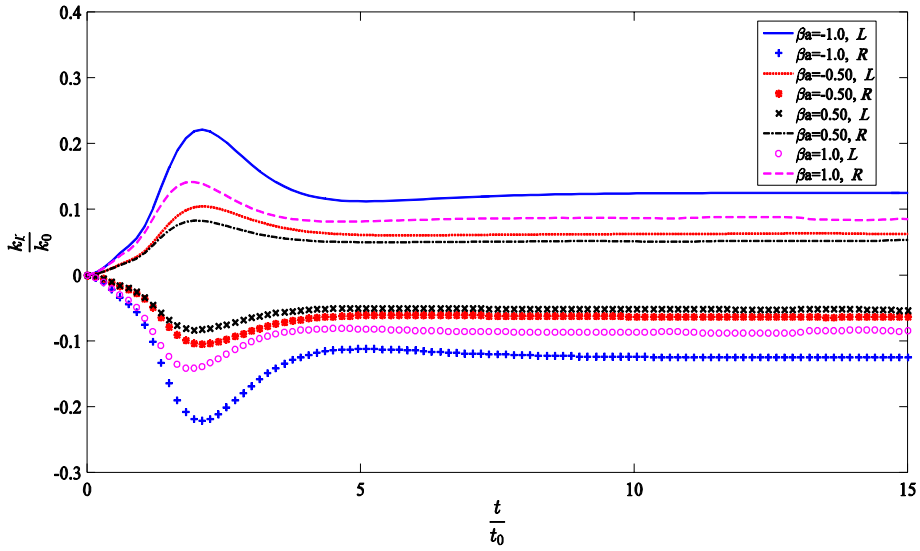

Fig. 8 Variations in normalized mode I transient DSIFs of a single interface crack for different dimensionless nonhomogeneity parameters under shear traction

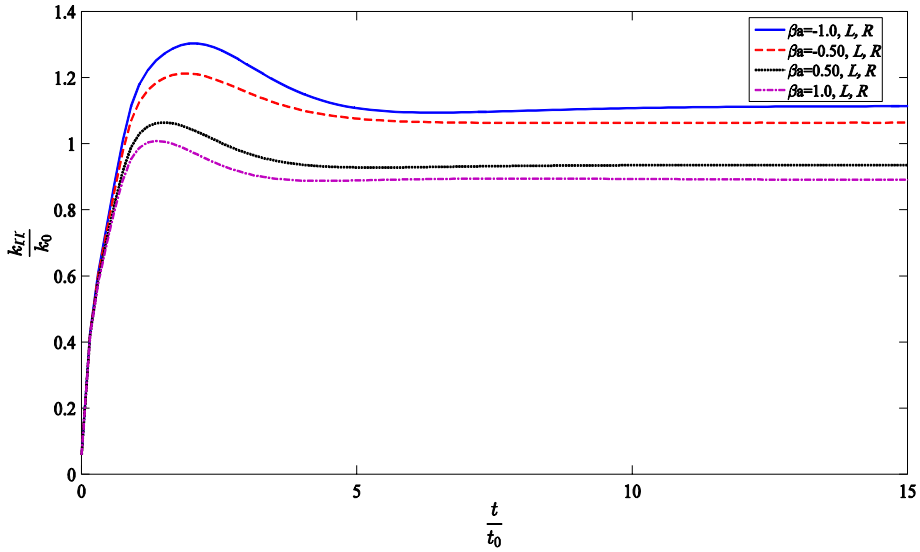

Fig. 9 Variations in normalized mode II transient DSIFs of a single interface crack for different dimensionless nonhomogeneity parameters under shear traction

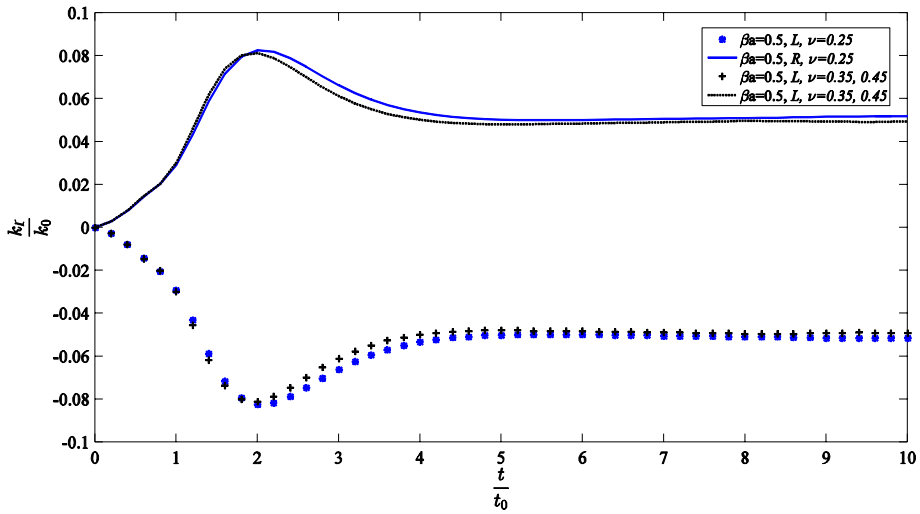

Fig. 10 Variations in normalized mode I transient DSIFs of a single interface crack for different Poisson's ratios under shear traction

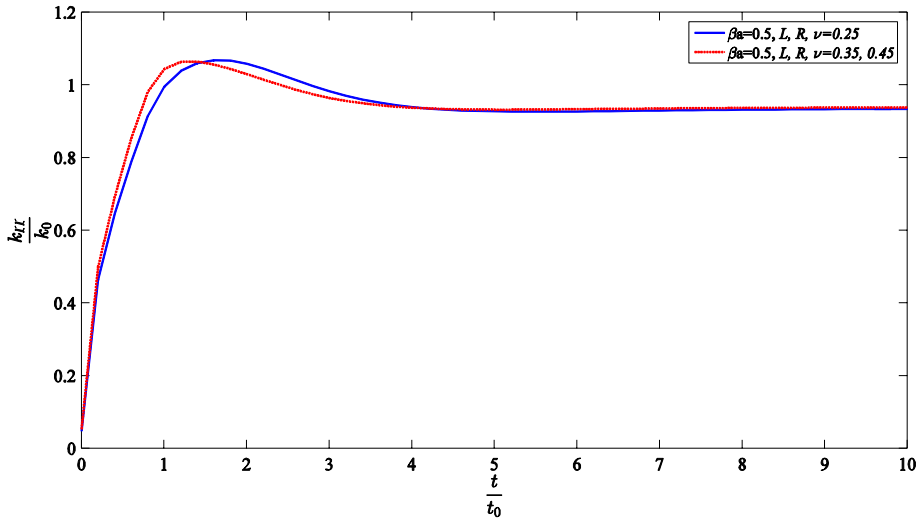

Fig. 11 Variations in normalized mode II transient DSIFs of a single interface crack for different Poisson's ratios under shear traction

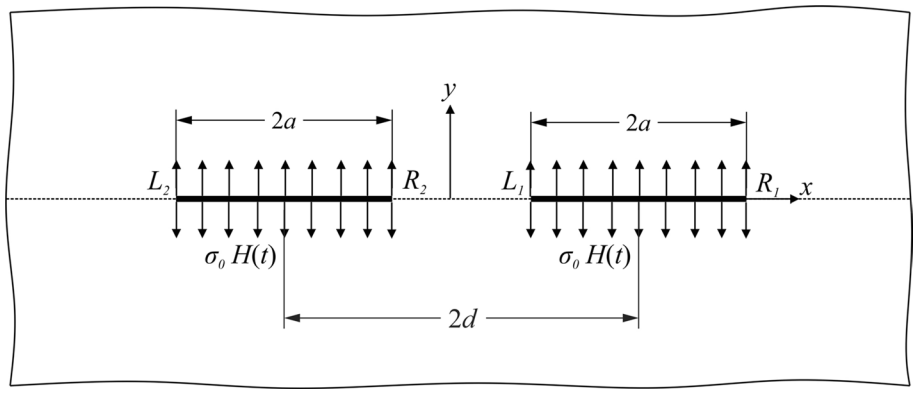

Fig. 12 Geometry of two cracks located between two dissimilar half-planes subjected to uniform normal step function

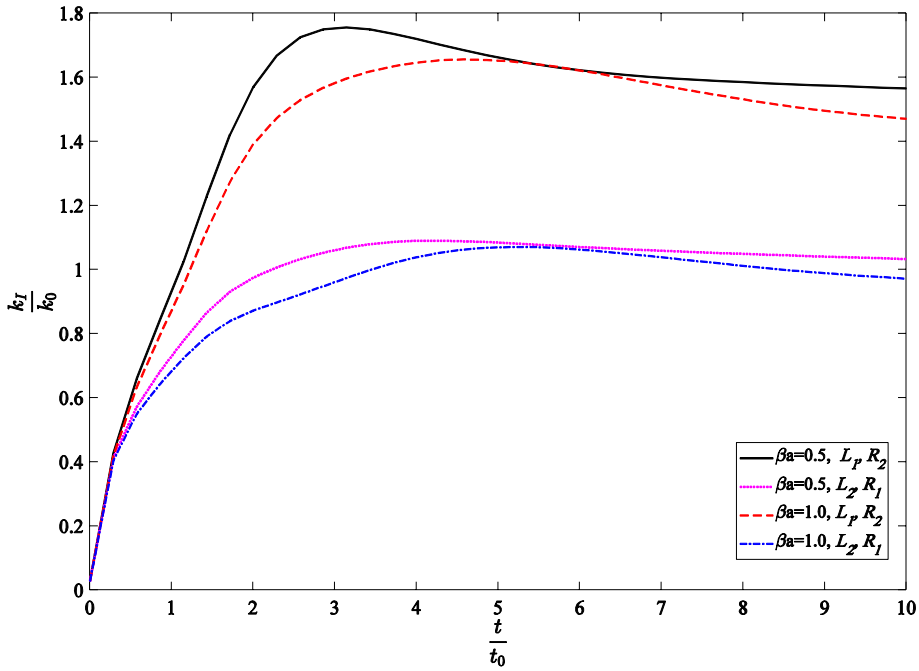

Fig. 13 Interaction of mode I of two interface cracks under normal step function traction

and II transient dynamic stress intensity factors versus the normalized size of crack for time $t = 3$ ms and nonhomogeneity parameter $\beta a = 0.5, 1.0$ are plotted in Figs. 15 and 16, respectively. The crack centers are fixed, whereas the crack lengths are changing with the same rates. As it may be observed, as crack size increases, the interaction at the tips L_1 and R_2 of the cracks increases; therefore, DSIFs at these tips increase rapidly while the variation in DSIFs at tips L_2 and R_1 is very small. It is worth mentioning that the lack of symmetry produces mode II DSIFs even where cracks are subjected to normal traction.

In the last example, three equal cracks with lengths $2a$ located between two dissimilar half-planes with identical center-to-center distance $d/a = 2.1$ are shown in Fig. 17. The variations in dimensionless modes I and II transient dynamic SIFs versus the dimensionless time for nonhomogeneity parameter $\beta a = 0.5$ are plotted in Figs. 18 and 19, respectively.

As the problem is symmetrical, the values of mode I dynamic stress intensity factors at tips L_1R_1, L_3R_2 and L_2R_3 are identical. It is found from Figs. 18 and 19 the dynamic stress intensity factor at tips of crack L_1R_1 is higher than that at the other tips.

5 Concluding remarks

The present work is an analytical method based on the distributed dislocation technique to calculate the transient mixed-mode stress intensity factors for multiple cracks located between two dissimilar half-planes. In this study, a single crack, two and three cracks have been selected for analyzing stress intensity factors at crack tips. The material properties in the nonhomogeneous medium are assumed to change continuously along the y-axis, and also crack faces are loaded by uniform normal and shear step function traction. The Fourier

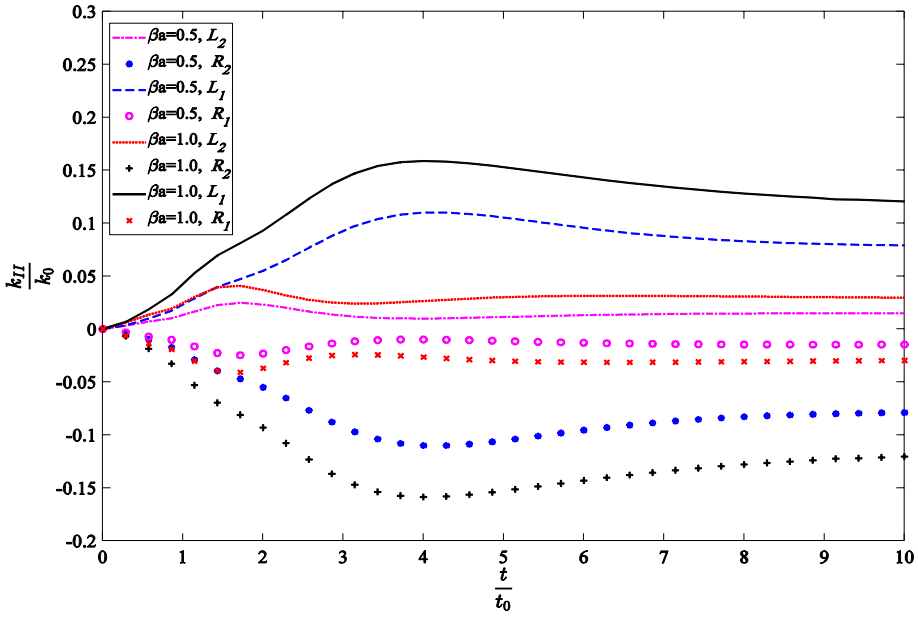

Fig. 14 Interaction of mode II of two interface cracks under normal step function traction

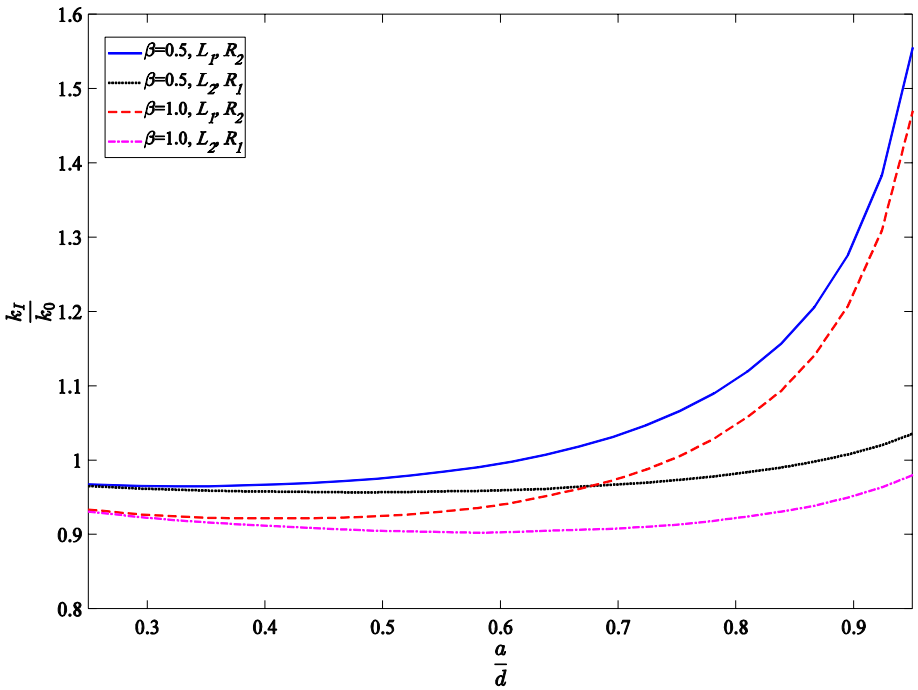

Fig. 15 Mode I normalized transient DSIFs versus crack sizing of two interface cracks under step function normal traction

and Laplace transforms are applied to reduce the problem to a system of singular integral equations with Cauchy-type singularity. These equations are then solved by the numerical Laplace technique and Lobatto–Chebyshev integration formula to obtain the dislocation density on the crack face.

The results reported in Sect. 4 indicate that the nonhomogeneity parameters have a significant influence on the transient dynamic stress intensity factors while the Poisson's ratio has only a negligible influence on the transient dynamic stress intensity factors. With the increase in the value of the βa, the upper side of the half-plane becomes stiffer and the mode I DSIF in normal loading and also mode II DSIFs in shear loading at the crack tip decrease regularly, as this process has been reported by Chen and Erdogan [29]. The values of DSIFs for two and three cracks are more of single crack because the interaction between crack tips in multiple cracks is greater than that of the single crack tip.

Appendix 1

Parameters that appeared in Eq. (14) are

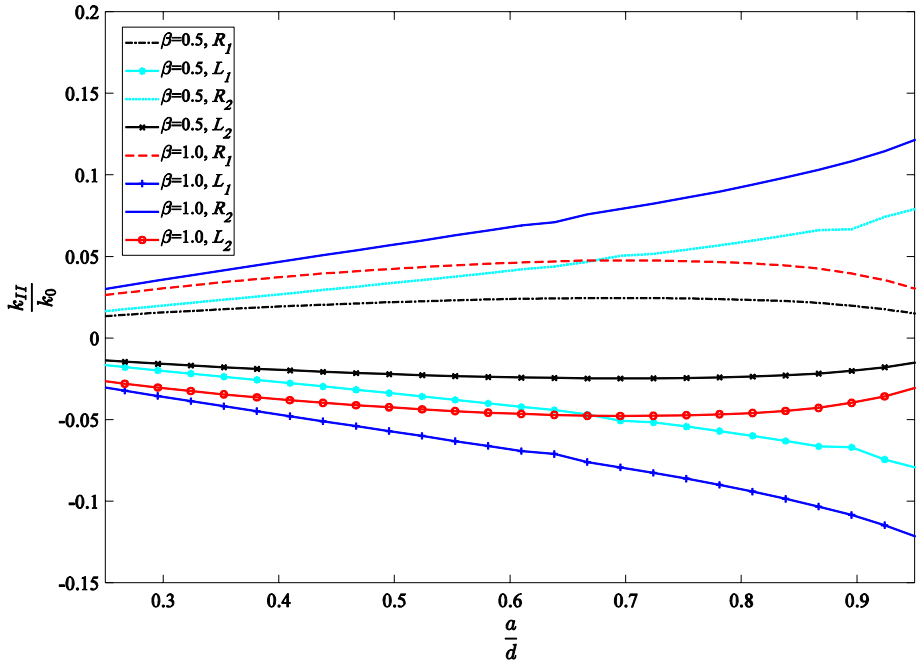

Fig. 16 Mode II normalized transient DSIFs versus crack sizing of two interface cracks under step function normal traction

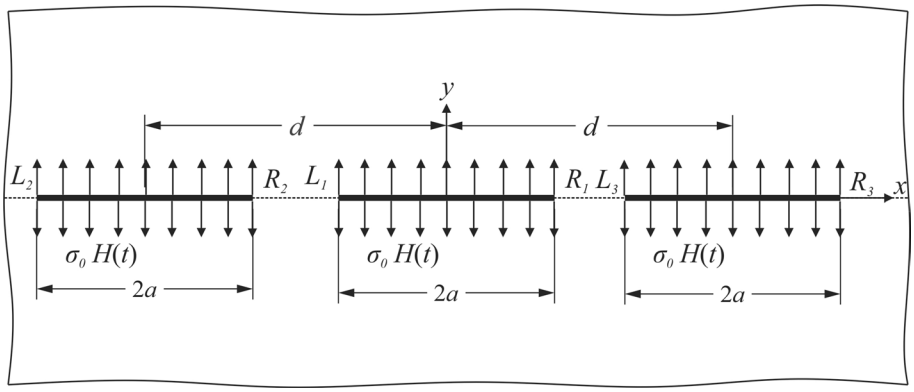

Fig. 17 Geometry of three cracks located between two dissimilar half-planes subjected to uniform normal step function

$$
\begin{aligned}
A_{11} &= [a_{24}(-b_{13}b_{21} + b_{11}b_{23}) + a_{23}(b_{14}b_{21} - b_{11}b_{24}) + a_{21}(-b_{14}b_{23} + b_{13}b_{24})]/\Delta,\\
A_{12} &= [a_{24}(-b_{13}b_{21} + b_{11}b_{23}) + a_{23}(b_{14}b_{21} - b_{11}b_{24}) + a_{21}(-b_{14}b_{23} + b_{13}b_{24})]/\Delta,\\
A_{21} &= -[a_{14}(-b_{13}b_{21} + b_{11}b_{23}) + a_{13}(b_{14}b_{21} - b_{11}b_{24}) + a_{11}(-b_{14}b_{23} + b_{13}b_{24})]/\Delta,\\
A_{22} &= -[a_{14}(-b_{13} + b_{23}) + a_{13}(b_{14} - b_{24}) + b_{13}b_{24} - b_{14}b_{23}]/\Delta,\\
C_{11} &= [a_{14}(a_{23}b_{21} - a_{21}b_{23}) + a_{13}(-a_{24}b_{21} + a_{21}b_{24}) + a_{11}(a_{24}b_{23} - a_{23}b_{24})]/\Delta,\\
C_{12} &= [a_{14}(a_{23} - b_{23}) + a_{13}(-a_{24} + b_{24}) + a_{24}b_{23} - a_{23}b_{24}]/\Delta,\\
C_{21} &= -[a_{14}(a_{23}b_{11} - a_{21}b_{13}) + a_{13}(-a_{24}b_{11} + a_{21}b_{14}) + a_{11}(a_{24}b_{13} - a_{23}b_{14})]/\Delta,\\
C_{22} &= -[a_{14}(a_{23} - b_{13}) + a_{13}(-a_{24} + b_{14}) + a_{24}b_{13} - a_{23}b_{14}]/\Delta,\\
\Delta &= a_{11}a_{24}b_{13} - a_{11}a_{23}b_{14} - a_{24}b_{13}b_{21} + a_{23}b_{14}b_{21} - a_{11}a_{24}b_{23} + a_{24}b_{11}b_{23} + a_{11}b_{14}b_{23}\\
&\quad - a_{21}b_{14}b_{23} + a_{14}[a_{23}(b_{11} - b_{21}) + b_{13}(-a_{21} + b_{21}) + b_{23}(a_{21} - b_{11})] +\\
&\quad + b_{24}[a_{23}(a_{11} - b_{11}) + (-a_{11} + a_{21})b_{13}] + a_{13}[b_{14}(a_{21} - b_{21}) + a_{24}(-b_{11} + b_{21}) + b_{24}(-a_{21} + b_{11})].
\end{aligned}
$$

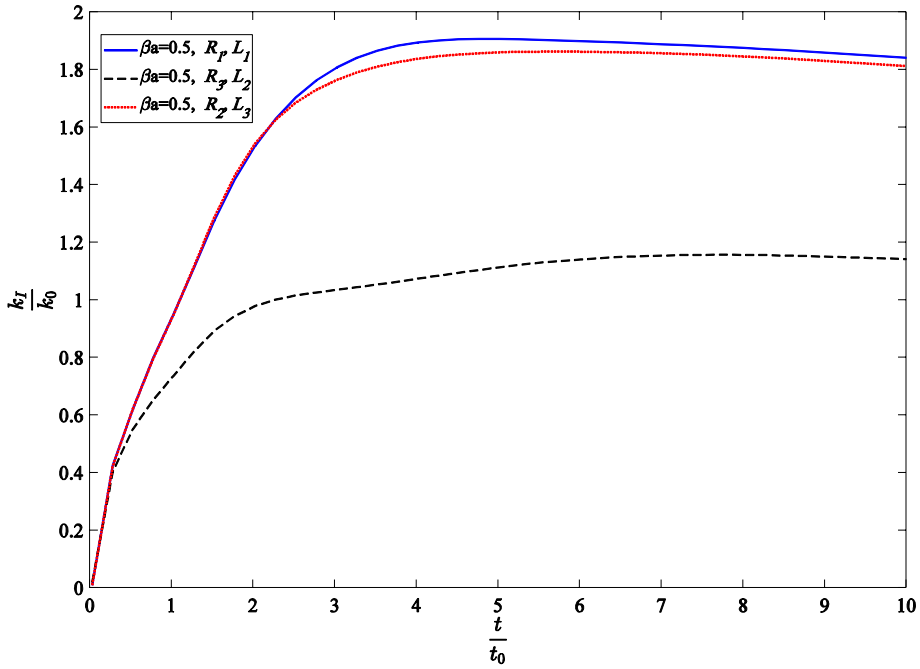

Fig. 18 Interaction of mode I of three interface cracks under normal step function traction

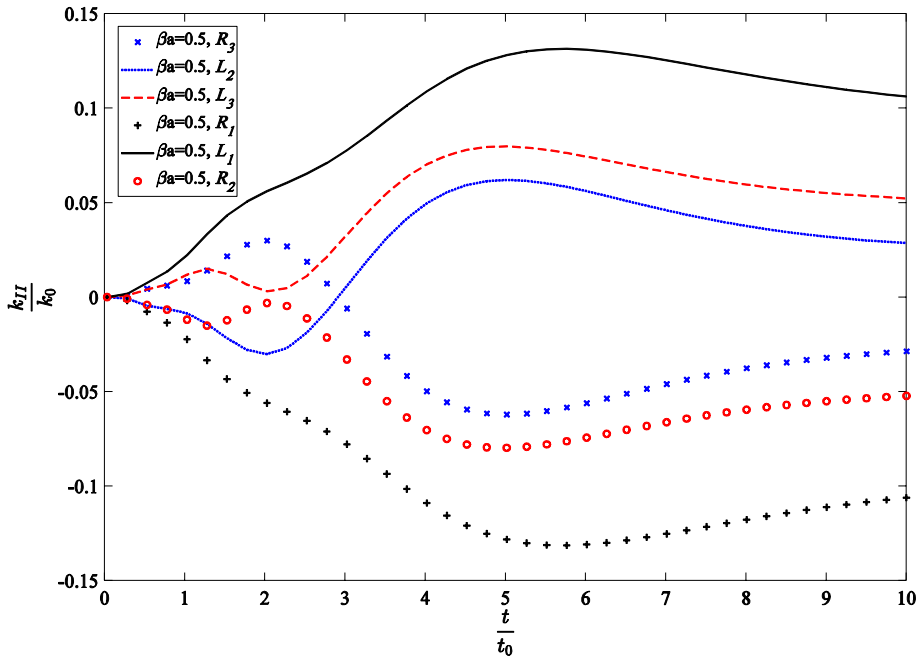

Fig. 19 Interaction of mode II of three interface cracks under normal step function traction

References

1. Delale F, Erdogan F (1988) On the mechanical modeling of the interfacial region in bonded half-planes. J Appl Mech 55(2):317–324
2. Hutchinson JW, Suo Z (1991) Mixed mode cracking in layered materials. Adv Appl Mech 29:63–191
3. Konda N, Erdogan F (1994) The mixed mode crack problem in a nonhomogeneous elastic medium. Eng Fract Mech 47(4):533–545
4. Itou S, Haliding H (1997) Dynamic stress intensity factors around two parallel cracks in an infinite-orthotropic plane subjected to incident harmonic stress waves. Int J Solids Struct 34(9):1145–1165
5. Ikeda T, Miyazaki N, Soda T (1998) Mixed mode fracture criterion of interface crack between dissimilar materials. Eng Fract Mech 59(6):725–735
6. Kadioğlu S, Dag S, Yahsi S (1998) Crack problem for a functionally graded layer on an elastic foundation. Int J Fract 94(1):63–77

7. Jiang L, Wang X (2002) On the dynamic crack propagation in an interphase with spatially varying elastic properties under inplane loading. Int J Fract 114(3):225–244
8. Chen J, Liu Z, Zou Z (2002) Transient internal crack problem for a nonhomogeneous orthotropic strip (Mode I). Int J Eng Sci 40(15):1761–1774
9. Feng W, Zhang Z, Zou Z (2003) Impact failure prediction of Mode III crack in orthotropic functionally graded strip. Theor Appl Fract Mech 40(1):97–104
10. Guo LC, Wu LZ, Ma L (2004) The dynamic fracture behavior of a functionally graded coating–substrate system. Compos Struct 64(3):433–441
11. Dag S, Yildirim B, Erdogan F (2004) Interface crack problems in graded orthotropic media: analytical and computational approaches. Int J Fract 130(1):471–496
12. Chen J, Liu Z (2005) Transient response of a mode III crack in an orthotropic functionally graded strip. Eur J Mech A Solids 24(2):325–336
13. Wang BL, Mai YW (2006) A periodic array of cracks in functionally graded materials subjected to transient loading. Int J Eng Sci 44(5):351–364
14. Dong LY, Bin J, Nan Z, Qiang TL, Yao D (2006) Dynamic stress intensity factor of the weak/micro-discontinuous interface crack of a FGM coating. Int J Solids Struct 43(16):4795–4809
15. Dag S, Ilhan KA (2008) Mixed-mode fracture analysis of orthotropic functionally graded material coatings using analytical and computational methods. J Appl Mech 75(5):051104
16. Itou S (2015) Dynamic stress intensity factors around three parallel cracks in an infinite medium during a passage of impact normal stresses. Acta Mech 226(7):2407
17. Itou S (1980) Transient response of a finite crack in a strip with stress-free edges. J Appl Mech 47(4):801–805
18. Monfared MM, Ayatollahi M (2016) Multiple crack problems in nonhomogeneous orthotropic planes under mixed mode loading conditions. Eng Fract Mech 155:1–17
19. Monfared MM, Bagheri R (2016) Multiple interacting arbitrary shaped cracks in an FGM plane. Theor Appl Fract Mech 86:161–170
20. Monfared MM, Ayatollahi M, Mousavi SM (2016) The mixed-mode analysis of a functionally graded orthotropic half-plane weakened by multiple curved cracks. Arch Appl Mech 86(4):713–728
21. Monfared MM, Bagheri R, Yaghoubi R (2018) The mixed mode analysis of arbitrary configuration of cracks in an orthotropic FGM strip using the distributed edge dislocations. Int J Solids Struct 130:21–35
22. Stehfest H (1970) Algorithm 368: numerical inversion of Laplace transforms [D5]. Commun ACM 13(1):47–49
23. Sourki R, Ilyaei S, Bastanfar M, Monfared MM (2018) Multiple cracks analysis in a FG orthotropic layer with FGPM coating under anti-plane loading. J Braz Soc Mech Sci Eng 40(6):309
24. Peyman S, Ghajar R, Irani S (2019) Computation of dynamic stress intensity factors for cracks in three-dimensional functionally graded solids. Proc Inst Mech Eng Part L J Mater Des Appl 233(5):862–873
25. Bueckner H (1958) The propagation of cracks and the energy of elastic deformation. Trans ASME Ser E 80(6):1225–1230
26. Baghestani AM, Fotuhi AR, Fariborz SJ (2013) Multiple interacting cracks in an orthotropic layer. Arch Appl Mech 83(11):1549–1567
27. Sih G, Embley G, Ravera R (1972) Impact response of a finite crack in plane extension. Int J Solids Struct 8(7):977–993
28. Mottale H, Monfared MM, Bagheri R (2018) The multiple parallel cracks in an orthotropic non-homogeneous infinite plane subjected to transient in-plane loading. Eng Fract Mech 199:220–234
29. Chen YF, Erdogan F (1996) The interface crack problem for a nonhomogeneous coating bonded to a homogeneous substrate. J Mech Phys Solids 44(5):771–787